European Journal of Radiology Open 10 (2023) 100459

Contents lists available at ScienceDirect

European Journal of Radiology Open

journal homepage: www.elsevier.com/locate/ejro

Original article

Imaging biomarkers to stratify lymph node metastases in abdominal CT – Is radiomics superior to dual-energy material decomposition?

Scherwin Mahmoudi [a,*], Vitali Koch [a], Daniel Pinto Dos Santos [a,b], Jörg Ackermann [c], Leon D. Grünewald [a], Inga Weitkamp [a], Ibrahim Yel [a], Simon S. Martin [a], Moritz H. Albrecht [a], Jan-Erik Scholtz [a], Thomas J. Vogl [a], Simon Bernatz [a,d]

[a] University Hospital Frankfurt, Department of Diagnostic and Interventional Radiology, Theodor-Stern-Kai 7, 60590 Frankfurt, Germany
[b] University Hospital Cologne, Department of Diagnostic and Interventional Radiology, Kerpener Str. 62, 50937 Cologne, Germany
[c] Department of Molecular Bioinformatics, Institute of Computer Science, Johann Wolfgang Goethe-University, Robert-Mayer-Str. 11-15, 60325 Frankfurt am Main, Germany
[d] Dr. Senckenberg Institute for Pathology, University Hospital Frankfurt, Goethe University Frankfurt am Main, 60590 Frankfurt am Main, Germany

HIGHLIGHTS

- Radiomics and DECT can be used for prediction of abdominal lymph node metastases.
- Radiomics seems to be superior to DECT material decomposition analysis.
- Quantitative image biomarkers may not be restricted to centers with DECT equipment.
- Radiomics may be used to automate stratification of unequivocal lymph nodes.

ARTICLE INFO

Keywords:
Lymph node metastasis
Radiomics
Machine Learning
Dual-energy computed tomography
Abdominal imaging
Oncology

ABSTRACT

Purpose: To assess the potential of radiomic features in comparison to dual-energy CT (DECT) material decomposition to objectively stratify abdominal lymph node metastases.
Materials and methods: In this retrospective study, we included 81 patients (m, 57; median age, 65 (interquartile range, 58.7–73.3) years) with either lymph node metastases (n = 36) or benign lymph nodes (n = 45) who underwent contrast-enhanced abdominal DECT between 06/2015–07/2019. All malignant lymph nodes were classified as unequivocal according to RECIST criteria and confirmed by histopathology, PET-CT or follow-up imaging. Three investigators segmented lymph nodes to extract DECT and radiomics features. Intra-class correlation analysis was applied to stratify a robust feature subset with further feature reduction by Pearson correlation analysis and LASSO. Independent training and testing datasets were applied on four different machine learning models. We calculated the performance metrics and permutation-based feature importance values to increase interpretability of the models. DeLong test was used to compare the top performing models.
Results: Distance matrices and t-SNE plots revealed clearer clusters using a combination of DECT and radiomic features compared to DECT features only. Feature reduction by LASSO excluded all DECT features of the combined feature cohort. The top performing radiomic features model (AUC = 1.000; F1 = 1.000; precision = 1.000;

Abbreviations: ADB, AdaBoost; AUC, Area under the curve; CT, Computed tomography; CTDI, Computed tomography dose index; DICOM, Digital Imaging and Communications in Medicine; DLP, Dose-length product; DECT, Dual-energy computed tomography; GLCM, Gray Level Co-occurrence Matrix; GLDM, Gray Level Dependence Matrix; GLRLM, Gray Level Run Length Matrix; GLSZM, Gray Level Size Zone Matrix; HU, Hounsfield Units; ICC, Intra-class correlation coefficient; ID, Iodine density; ID%, Normalized iodine uptake; LR, Logistic Regression; mGy, Milligray; NGTDM, Neighboring Gray Tone Difference Matrix; PET, Positron emission tomography; RF, Random Forest; ROC, Receiver operating characteristics; ROI, Region of interest; SGB, Stochastic Gradient Boosting; VOI, Volume of interest.

* Corresponding author.
E-mail addresses: scherwin.mahmoudi@kgu.de (S. Mahmoudi), vitali.koch@kgu.de (V. Koch), daniel.pintodossantos@kgu.de (D.P.D. Santos), j.ackermann@bioinformatik.uni-frankfurt.de (J. Ackermann), leondavid.gruenewald@kgu.de (L.D. Grünewald), ingaweitkamp@gmx.de (I. Weitkamp), ibrahim.yel@kgu.de (I. Yel), simon.martin@kgu.de (S.S. Martin), moritz.albrecht@kgu.de (M.H. Albrecht), jan-erik.scholtz@web.de (J.-E. Scholtz), thomas.vogl@kgu.de (T.J. Vogl), simon.bernatz@kgu.de (S. Bernatz).

https://doi.org/10.1016/j.ejro.2022.100459
Received 29 September 2022; Received in revised form 16 November 2022; Accepted 30 November 2022
Available online 9 December 2022

Random Forest) was significantly superior to the top performing DECT features model (AUC = 0.942; F1 = 0.762; precision = 0.800; Stochastic Gradient Boosting) (DeLong < 0.001).
Conclusion: Imaging biomarkers have the potential to stratify unequivocal lymph node metastases. Radiomics models were superior to DECT material decomposition and may serve as a support tool to facilitate stratification of abdominal lymph node metastases.

1. Introduction

Lymphadenopathy has a wide range of differential diagnoses, including infectious disease, benign inflammatory processes or malignancy [1]. In computed tomography (CT), the assessment of pathological lymph nodes is primarily based on lymph node size and the subjective evaluation of morphologic criteria, including shape, internal texture, and presence of fatty hilum [2]. Larger lymph nodes are more likely considered to be suspicious [2,3], but a definite diagnosis of lymph node involvement in suspected or confirmed malignancy remains difficult in cases with equivocal lymph node size and morphology [4,5]. To achieve acceptable levels of specificity and sensitivity (84.4 %; 73.5 %), a threshold of 1.5 cm short-axis transverse diameter for pathological lymph nodes is proposed [3].

The early identification of patients with lymph node metastases is crucial and has therapeutic and prognostic relevance. At the same time, radiologists are confronted with an increasing workload as the demand for medical imaging is growing [6]. Quantitative image analysis tools such as dual-energy CT (DECT) post-processing and radiomics may have the potential to non-invasively stratify patients with lymph node metastases and consequently facilitate clinical decision-making.

DECT provides a wide range of post-processing techniques including material decomposition analysis. Some of these methods have been increasingly implemented into clinical routine [7,8]. A potential application of DECT material decomposition is iodine-selective mapping which visualizes the contrast agent iodine in standard DECT series [9]. Iodine-selective imaging allows for further tissue characterization compared to visual-descriptive reporting as the blood supply can be quantitatively depicted in tumor entities [9]. The potential benefits of lymph node iodine quantification have been assessed in recent studies, suggesting lower iodine concentration in lymph node metastases compared to benign lymph nodes [10,11]. Nevertheless, these studies followed a rather comparative approach without applying and testing advanced bioinformatic prediction models.

Radiomics is a technique based on high-dimensional quantitative image analysis and has emerged as a non-invasive research tool to characterize tissue morphology beyond visual perception [12]. The computational technique may provide surrogate information on pathophysiological and biochemical processes [12]. Particularly in the field of oncology, radiomics seems promising as the features provide additional, high dimensional data that may facilitate non-invasive stratification of tumor subtypes, treatment response and clinical outcome [13–15].

DECT material decomposition and radiomics have shown promising results in the non-invasive characterization of abdominal lymph nodes beyond standard-of-care reading and reporting in patients with gastric cancer, colorectal carcinoma, and pancreatic carcinoma [16–18]. The application of imaging biomarkers may have the potential to aid clinical decision making [12,19]. Yet, it is unclear, whether the combined application of both DECT and radiomics may further improve the diagnostic accuracy for the prediction of lymph node metastases. Therefore, the aim of our study was to analyze the potential of imaging biomarkers to objectively identify unequivocal lymph node metastases in a broad spectrum of patients with different primary tumors. As radiologists are increasingly confronted with a growing workload, the use of imaging biomarkers as a prioritization tool might enable radiologists to focus on equivocal cases [6]. We aimed to stratify the most reliable radiomic features and DECT features for abdominal lymph node metastases prediction to improve the interpretability of our models. Further, we hypothesized that a combined application of both techniques may improve the prediction of lymph node metastases in contrast-enhanced abdominal CT compared to DECT features only.

2. Material and methods

The local Ethics committee of our institution approved this retrospective study (project number: 20–688) and waived informed written consent.

2.1. Study design

A total of 81 patients with lymph node metastases (n = 36) and benign lymph nodes (n = 45) who underwent contrast-enhanced abdominal DECT imaging between 06/2015 and 07/2019 were included in the study.

Inclusion criteria for the metastasis cohort were: (I) > 18 years of age, (II) confirmation of lymph node metastasis by histopathology (lymphadenectomy or lymph node biopsy), PET-CT or follow-up imaging, (III) unequivocal lymph node metastasis according to RECIST criteria [3], (IV) abdominal DECT imaging with availability of 1.5 mm low and high kV series. If follow-up imaging was used as reference-standard, lymph nodes were defined as malignant when progressive disease was stated in the follow-up according to RECIST criteria and lymph node size was progressive or when partial/complete response was diagnosed according to RECIST criteria and lymph node size was regressive under systemic therapy [3].

Exclusion criteria were: (I) patients with multiple diagnosed malignancies, (II) imaging artifacts. The inclusion and exclusion criteria for the control (benign) cohort differed in inclusion point (II) and (III) to not have confirmed lymph node metastases. Further, only patients without diagnosis of abdominal malignancy were included into the control cohort. In cases of patients with multiple CT studies, the baseline DECT scan was taken for analysis.

All clinical data were obtained in clinical routine. Detailed patient characteristics are depicted in Table 1. Fig. 1 shows the flowchart of patient inclusion following Standards for Reporting Diagnostic Accuracy Studies (STARD).

2.2. CT acquisition protocol

All examinations were performed using a third-generation, dual-source, dual-energy CT system (Somatom Force, Siemens Healthineers). The acquisition protocol operated the x-ray tubes at different kilovoltage and tube current settings (tube A: 100 kV, 190 mAs; tube B: Sn150 kV, 95 mAs). An additional tin filter (Selective Photon Shield II, Siemens Healthineers) was used in tube B to reduce radiation exposure. The dual-energy protocol (craniocaudal direction; rotation time, 0.5 s; pitch, 0.6; collimation, 2 ×192 x 0.6) included automatic attenuation-based tube current modulation (CARE Dose 4D, Siemens Healthineers). Contrast media injection was performed through a peripheral vein of the forearm at a flow of 2–3 ml/s. A non-ionic contrast agent (Imeron® 400 mg iodine/ml; Bracco, Milan, Italy) with a total of 1.2 ml/kg body weight (maximum of 120 ml) was administered. Image acquisition during venous phase of contrast enhancement started 70 s after contrast agent injection in inspiratory breath-hold. CT dose index (CTDI) and dose-length-product (DLP) were recorded. Iterative reconstruction algorithm (ADMIRE®, Siemens Healthineers, Strength Level 3) was used for

Table 1
Patient characteristics.

Parameters	*Lymph node metastasis*	*Benign lymph nodes*
Number of patients (n)	36	45
Male / Female (n)	25 / 11	32 / 13
Age (median years)	63 (34 – 81)	67 (47 – 87)
Mean attenuation (HU) and SD of the respective lymph nodes	70.54 ± 29.95	62.91 ± 31.75
Mean CTDI (mGy)	8.5 ± 5.0 (2.3 – 30.3)	8.7 ± 4.0 (2.7 – 26.7)
Mean DLP (mGy*cm)	439.8 ± 330.9 (88.6 – 1823.9)	592.1 ± 304.2 (96.5 – 1970.4)
Lymph node entity		–
RCC	6	
Urothelial carcinoma	6	
Prostate cancer	4	
Pancreatic cancer	4	
CRC	3	
Malignant melanoma	3	
CCC	2	
Gastric cancer	1	
HCC	1	
NSCLC	1	
Vaginal squamous cell carcinoma	1	
Testicular cancer	1	
Mammary carcinoma	1	
Ovarian cancer	1	
AEG	1	

If not depicted otherwise, the numbers without parenthesis depict absolute numbers. Data in round parenthesis are the min/max values. AEG, adenocarcinoma of esophagogastric junction; CCC, cholangiocellular carcinoma; CTDI, computed tomography dose index; CRC, colorectal cancer; DLP, dose-length product; HCC, hepatocellular carcinoma; mGy, milligray; NSCLC, non-small-cell lung carcinoma; RCC, renal cell carcinoma; SD, standard deviation.

image reconstruction.

2.3. Image preprocessing

DECT images were reconstructed in axial orientation (slice thickness, 1.5 mm; increment, 1.2 mm) with a dedicated dual-energy medium-soft convolution kernel (Qr40, advanced model-based iterative reconstruction [ADMIRE] level of 3).

DECT material decomposition image reconstruction was performed on a 3D multi-modality workstation (syngo.via, version VB10B, Siemens Healthineers). An iodine subtraction algorithm (Liver VNC, Siemens Healthineers) was used for material decomposition including iodine density (ID), normalized iodine uptake (ID%) and fat fraction (FF). ID% was calculated using the following formula: $ID\% = ID_{\text{lymph node}} / ID_{\text{aorta}}$. Region of interest (ROI) measurements for ID_{aorta} were performed manually in the abdominal aorta at the level of the celiac trunk. For radiomic analysis, the image stack was exported in Digital Imaging and Communications in Medicine (DICOM) format and imported into the 3D Slicer software platform (http://slicer.org, version 4.9.0) to visualize and process the DICOM image stack [20,21]. No further image manipulation was done as the Imaging Biomarker Standardization does not cover image preprocessing [22].

2.4. Image segmentation

One investigator (radiologist in training, 3 years of experience in oncology imaging) who had access to clinical data (histopathology, PET-CT or follow-up imaging) selected and marked three lymph nodes per patient. ROI and spheric volume of interest (VOI) circumscription for segmentation was manually performed by three investigators (I, especially trained investigator, 1 year of experience in oncology imaging; II, radiologist in training, 3.5 years of experience in oncology imaging; III, radiologist in training, 2 years of experience in oncology imaging) who were blinded to the clinical records. Each investigator segmented one of the three marked lymph nodes.

Three segmentations, each of a different independent lymph node, were obtained per patient. In total, 243 lymph nodes (lymph node metastases, n = 108; benign lymph nodes, n = 135) were segmented. ROI measurements for DECT analysis (Fig. 2) and VOI measurements for radiomic analysis (Fig. 3) were drawn as large as possible with a maximum diameter of 1.0 cm, carefully avoiding surrounding structures, calcifications and visual artifacts. We chose a maximum diameter of 1.0 cm to exclude potential shape bias between enlarged metastatic and small benign lymph nodes. The segmentations were independently reviewed by a board-certified and blinded radiologist (8 years of experience in oncology imaging) and no disagreement was stated.

2.5. Radiomic analysis

We used the open-source extension PyRadiomics within the 3D Slicer software platform to extract the radiomic features [21,23]. With default settings, we extracted all original standard features for each segmentation (n = 107, feature classes = 7): Shape, First Order Statistics, Gray Level Co-occurrence Matrix (GLCM), Gray Level Run Length Matrix (GLRLM), Gray Level Size Zone Matrix (GLSZM), Gray Level Dependence Matrix (GLDM), Neighboring Gray Tone Difference Matrix (NGTDM) [24]. We excluded the shape features (n = 14) for the following analyses as we used spheric VOIs. We calculated the radiomics quality score for our study and yielded a score of 12 (https://radiomics.world/rqs, supplementary material S4) [25].

2.6. Inter-observer robustness and feature redundancy

We calculated the intra-class correlation coefficient (ICC) for each feature and DECT material decomposition by defining each of the three independently segmented and measured lymph nodes per patient as one measurement and then calculating the ICC for these three measurements to assess the measurement's reproducibility [26]. We followed this approach as we aimed to analyze the texture's robustness on a patient level. We used ICC3 of the Pingouin package in Python [27]. ICC was interpreted with thresholds commonly used in radiomics research: ICC 0.75–1 = excellent, ICC 0.60–0.74 = good, ICC 0.40–0.59 = moderate, ICC$\leq$ 0.39 = poor [26]. For further analysis, we discarded all radiomic features with ICC$<$ 0.6 to include only radiomic features with at least good reproducibility (n = 31) and we excluded DECT features with ICC $\leq$ 0.39 (poor; Iodine Density) as not a single DECT feature had an ICC$\geq$ 0.6 (Supplementary Data S1). The robust features were inter-correlated by Pearson method and we excluded all highly correlated (Pearson $>$ 0.95) redundant features (n = 13) except one (Supplementary Data S2).

2.7. Imaging biomarkers to predict lymph node malignancy

We performed all analysis in Python 3.7.6, within Jupyter Notebook [28] and respective open-source packages to ensure transparency and sustainability. We aimed to predict our target variable (lymph node metastasis) either using DECT material decomposition, combined DECT and radiomic features or radiomic features only. Therefore, we stratified our independent variables into three feature groups: I, DECT feature group; II, combined feature group and III, radiomic feature group. First, we performed explorative data analysis on our datasets using euclidean distance matrices to explore the pairwise dataset relations and low dimensional embedding with t-SNE plots to explore cluster distributions (scikit-learn [29]). Next, we used Least absolute shrinkage and selection operator (LASSO) [29] to reduce the amount of features and the risk of overfitting. LASSO excluded all DECT features in the combined feature group, therefore the radiomic feature group and combined feature group yielded identical non-zero LASSO features and we respectively dismissed one redundant feature group (combined feature group) for

further analysis. The DECT-cohort had only two features and we did not perform LASSO for further feature reduction.

We drew 70 % random data samples as training set and used the remaining 30 % to test our model. We used StandardScaler [29] to scale the data to uniform variance. Next, we trained and tested four individual and independent machine learning models [29]: I, logistic regression classifier, II, AdaBoost classifier, III, Gradient Boosting classifier and IV, random forest classifier (see Supplementary Data S3 for detailed information on feature selection and machine learning models). For each classifier, we calculated the mean feature importance by repeating a shuffled permutation-based analysis of feature importance 15 times using the test dataset. We calculated the receiver operating characteristics (ROC) area under the curve (AUC), F-score and precision-score for each model using the test dataset and depict the respective ROC curves. We used the implementation of the WORC.statistics package [30] for the DeLong's test [31].

3. Results

3.1. Study population

The study population comprised 81 patients (57 male; median age 65 (interquartile range (IQR), 58.7–73.3) years) who underwent contrast-enhanced abdominal CT on the same DECT scanner. 36 patients (25 male; median age 63 (IQR, 55.2 – 72.0) years) were diagnosed with visually unequivocal lymph node metastases. The diagnosis was confirmed with histopathological analysis (lymph node biopsy, n = 7; lymphadenectomy, n = 2), PET/CT (n = 2) or follow-up CT scans

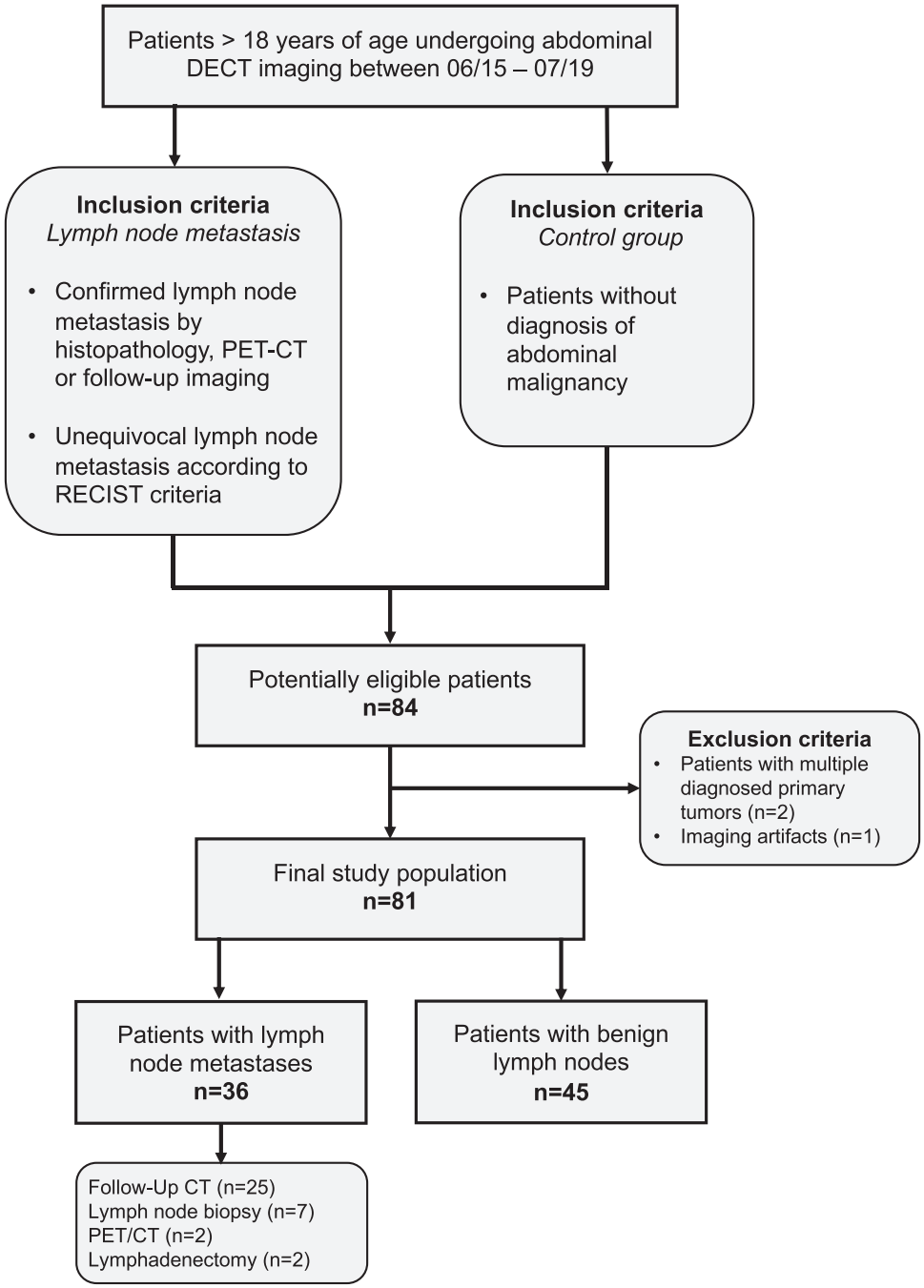

Fig. 1. STARD flowchart of study inclusion.

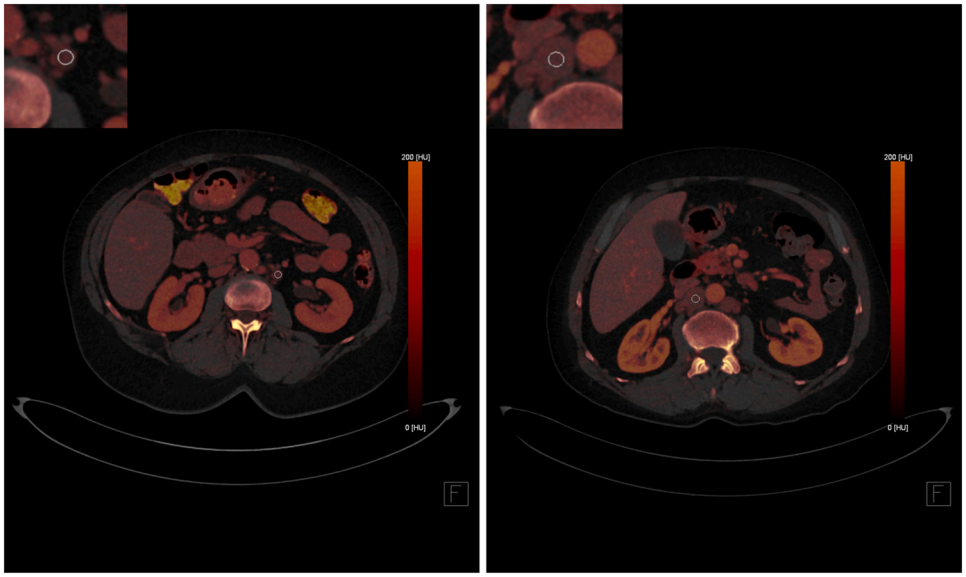

Fig. 2. Illustration of DECT iodine quantification segmentation. Axial DECT based iodine map images with region of interest (ROI) measurements of the respective lymph nodes. Left: 62-year-old female patient without abdominal malignancy. Right: 66-year-old male patient with prostate cancer with lymphogenic metastasis.

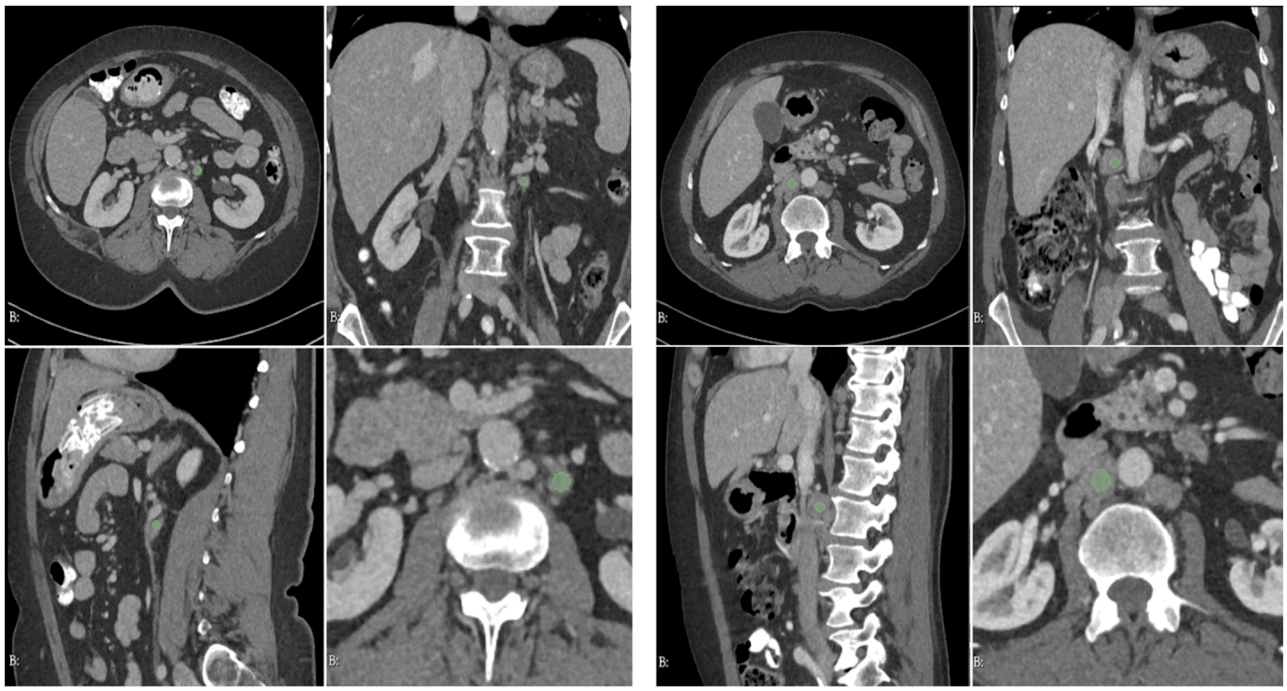

Fig. 3. Illustration of radiomics segmentation. Axial, coronal, sagittal and scaled up axial DE-CT images with standard volume of interest (VOI) measurements of the respective lymph nodes. Left: 62-year-old female patient without abdominal malignancy. Right: 66-year-old male patient with prostate cancer with lymphogenic metastasis.

(n = 25). The control group consisted of 45 patients who did not have malignant abdominal lymph nodes (32 male; median age 67 (IQR, 59.9 – 74.5) years). Detailed patient characteristics are depicted in Table 1.

Radiation metrics in venous phase acquisition were 8.6 ± 4.5 mGy (range, 2.3–30.3 mGy) for mean volume CTDI and 523.6 ± 323.6 mGy*cm (range, 88.6 mGy*cm – 1970.4 mGy*cm) for mean DLP.

3.2. Unsupervised cluster analysis

The pairwise euclidean distance for each sample is depicted in the distance matrices (Fig. 4A/B). With DECT features only, a stratification into two clusters might be presumed (Fig. 4A). The combined image post-processing techniques (DECT and radiomic features) revealed two definite distinct clusters (Fig. 4B). We could corroborate the finding in the respective t-SNE plots which depict lymph node metastases in orange (label = 1) and benign lymph nodes in blue (label = 0). The DECT features revealed no definite two clusters with a broad border of uncertainty (Fig. 4C). Two distinct clusters were seen in the combined cohort with only two outliers (Fig. 4D).

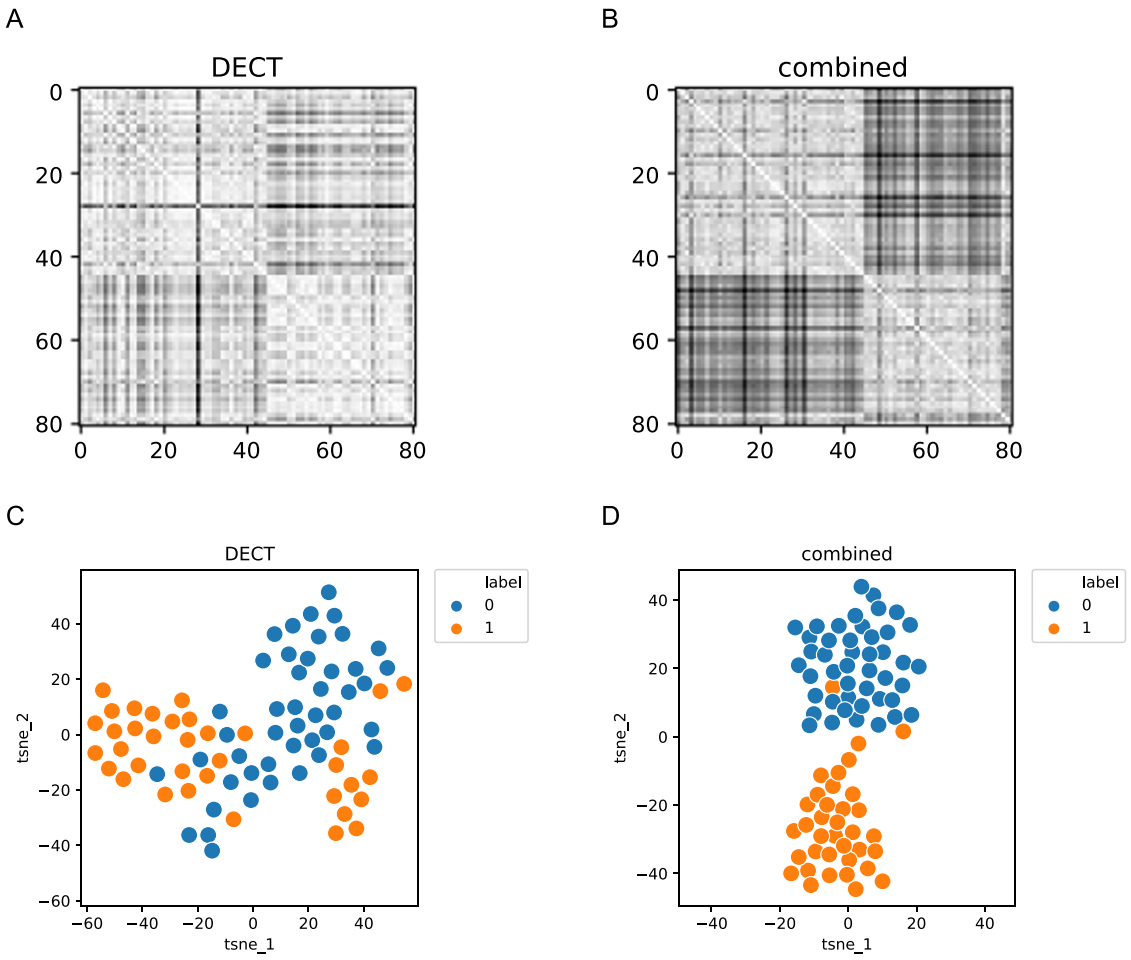

Fig. 4. Unsupervised explorative data analysis. Euclidean distance matrices with samples sorted by label (metastasis vs. benign) for the DECT (A) and combined feature cohort (B). White coloring represents smaller euclidean distances. Squarish patterns along the white diagonal reveal cluster with similar pairwise distance. In C) and D) t-SNE plots of the DECT and combined cohort depict the two-dimensional embedding of the joint probabilities (label: 1 (orange), metastasis; 0 (blue), benign). DECT, dual-energy computed tomography; t-SNE, t-distributed stochastic neighbor embedding.

3.3. Feature importance characteristics

LASSO was used to reduce the amount of radiomic features from 18 robust and non-redundant features (ICC $>$ 0.6 and Pearson $\leq$ 0.95, see supplementary data S1 and S2) to our final radiomic features set of 5 features.

The final features were part of the feature classes firstorder (n = 1), GLDM (n = 2) and GLSZM (n = 2). We calculated the permutated feature importance for each model. Within the DECT features, fat fraction was superior to ID% in all models. In the radiomics feature group, two features (LargeDependenceEmphasis, LargeAreaEmphasis) yielded non-zero importance values in all four independent models. Details of permutation-based feature importance analysis for each model are depicted in Table 2.

Table 2
Permutation-based feature importance analysis for each model.

	Class	LR		ADB		SGB		RF	
Radiomics		*Imp*	*Std*	*Imp*	*Std*	*Imp*	*Std*	*Imp*	*Std*
Energy	firstorder	-0.005	0.014	0.000	0.000	0.000	0.000	0.027	0.019
Dependence NonUniformity	GLDM	0.000	0.021	0.000	0.000	0.032	0.026	0.027	0.019
LargeDependence Emphasis	GLDM	0.059	0.048	0.035	0.025	0.003	0.010	0.003	0.010
LargeArea Emphasis	GLSZM	-0.019	0.020	0.373	0.075	0.029	0.023	0.029	0.023
LargeAreaHigh GrayLevelEmphasis	GLSZM	-0.024	0.020	-0.021	0.025	0.024	0.020	0.000	0.000
DECT									
Iodine_Density_%	–	-0.021	0.035	-0.003	0.042	-0.008	0.016	-0.013	0.019
Fat_Fraction	–	0.253	0.107	0.205	0.092	0.248	0.093	0.243	0.098

Final feature set after LASSO feature reduction of the 18 robust and non-redundant features and DECT feature set. ADB, AdaBoost; GLDM, Gray Level Dependence Matrix; GLSZM, Gray Level Size Zone Matrix. LR, logistic regression; RF, Random Forest; SGB, Stochastic Gradient Boosting. The LR feature importance of DependenceNonUniformity was 1.480e-17 and therefore 0.000 is shown in the table with a non-zero Std.

3.4. Model performance differences and best performing model comparison

In the DECT feature group, performances from AUC = 0.756 (F1 = 0.727; ADB) up to AUC = 0.942 (F1 = 0.762; SGB) were achieved (Fig. 5A).

The radiomics feature group revealed performances from AUC = 0.919 (F1 = 0.909) (ADB) up to AUC = 1.000 (F1 = 1.000; SGB and RF) (Fig. 5B).

In Table 3 we depict detailed performance characteristics. Fig. 6 shows the best performing models of each cohort (SGB, DECT; RF, radiomics) with superior performance of the radiomics feature group RF model (DeLong $p < 0.001$).

4. Discussion

The aim of this retrospective study was to compare the potential of radiomic features versus DECT-based material decomposition analysis to identify abdominal lymph node metastases and to stratify the best working model and most important features. The results of our study showed that radiomics-based machine learning models of CT images were superior to DECT-based material decomposition analysis techniques for the identification of abdominal lymph node metastases in contrast-enhanced CT. Therefore, quantitative image biomarkers may not be restricted to centers with DECT equipment as high performing artificial intelligence methodologies are applicable in standard-of-care CT images.

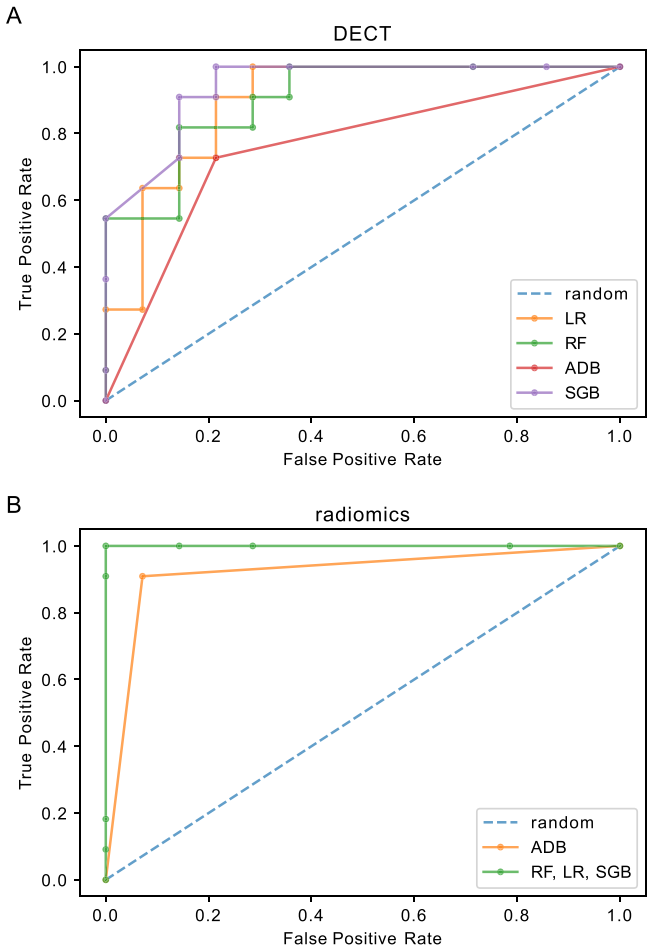

Fig. 5. Performance visualization by receiver operating characteristics curves. Receiver operating characteristics (ROC) curves are depicted for the DECT (A) and radiomics (B) feature group. Each model is color coded. Some models revealed identical performances and respectively identical ROC curves (see Table 3). LR, Logistic regression; RF, Random Forest; ADB, AdaBoost; SGB, Stochastic Gradient Boosting.

Our findings indicate that the automatic stratification of unequivocal lymph node metastases based on radiomic features can serve as a prioritization support tool to help radiologists focus on unequivocal and critical cases.

The identification of patients with lymph node metastases is decisive and has therapeutic and prognostic relevance [32,33]. RECIST criteria give guidance, but follow-up scans may be necessary for diagnosis, potentially causing delayed detection of nodular spread or recurrence of disease. Positron emission tomography (PET) CT may confirm a suspected nodal involvement but high radiation exposure and costs require restrictive application [34]. Over recent years, the application of DECT post-processing techniques and radiomics has become an evolving research field, leading to improved non-invasive lesion characterization. Particularly in cancer research, radiomics is a rapidly evolving research field [12]. In contrast to basic material decomposition analysis techniques, radiomics can provide additional, higher dimensional data by extracting a variety of mineable image features. Several studies have investigated the impact of DECT based material decomposition analysis and radiomic features for tissue and tumor characterization [35–37]. In a recent study, the authors investigated the potential of both DECT based iodine quantification and radiomics to differentiate normal liver tissue, hepatic steatosis and liver cirrhosis [38]. In accordance with our results, radiomics showed slightly better performance compared to DECT material decomposition. Similar findings were presented in oncology imaging: In two recently published studies, the authors verified statistical differences of DECT based iodine quantification parameters and radiomic features in benign and malignant liver lesions and pancreatic lesions [36,37]. The findings of these studies are in line with our results, suggesting a slightly better performance of radiomic features compared to DECT based material decomposition analysis techniques. Furthermore, several studies have specifically investigated the impact of DECT features on the characterization of lymph nodes [39,40]. In accordance with the findings of Rizzo et al. and Li et al., our data confirms lower DECT derived iodine concentration in lymph node metastases compared to benign lymph nodes [39,40]. An efficient predictability for lymph node metastases has also been confirmed for radiomic features. For example, in the field of abdominal imaging, the potential of deep learning radiomics has been validated for the prediction of lymph node metastases in pancreatic cancer and gastric cancer [41,42]. In our study, we revealed superior predictive performance of machine learning models trained with radiomic features compared to training with DECT material decomposition values. Radiomic features showed higher robustness than DECT material decomposition and they seem to have more comprehensive and complementary value in comparison with DECT features.

One major advantage of radiomics compared to DECT based algorithms is that it can be applied in standard-of-care CT scans without the need for DECT equipment. As DECT is not yet as widely used as single-energy CT, DECT material decomposition analysis techniques are restricted to a minor group of well-equipped healthcare centers. However, radiomics offers a superior data characterization tool that is accessible to a very wide hospital spectrum.

Our study has several limitations, which have to be taken into account. As a retrospective single center study, the sample size is modest and may lead to case selection bias. Our study includes 81 patients, and a larger cohort might have been favorable. This might reduce generalizability of the result.

Even if DECT equipment is accessible, retrospective application of DECT post-processing is limited to cases where particular image series such as DECT raw data (1.5 mm low and high kV series) are available for material decomposition analysis. However, availability of these data is not always given due to storage capacity reasons. This limitation restricts the use of DECT material decomposition analysis to selected

Table 3
Model performance metrics.

	LR		ADB		SGB		RF	
	Radiomics	*DECT*	*Radiomics*	*DECT*	*Radiomics*	*DECT*	*Radiomics*	*DECT*
AUC	1.000	0.896	0.919	0.756	1.000	0.942	1.000	0.903
F1	0.900	0.783	0.909	0.727	1.000	0.762	1.000	0.762
Prec	1.000	0.750	0.909	0.727	1.000	0.800	1.000	0.800

ADB, AdaBoost; AUC, area under the curve; LR, logistic regression; Prec, precision; RF, Random Forest; SGB, Stochastic Gradient Boosting.

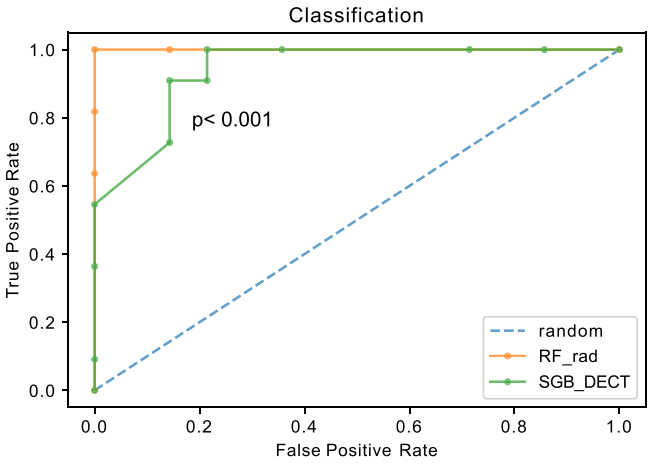

Fig. 6. Comparison of the top performing models. Receiver operating characteristics (ROC) curves of the top performing model of the DECT (Stochastic Gradient Boosting, SGB, green) and radiomic (Random Forest, RF, orange) feature group with DeLong test (*p*-value) for statistical analysis.

cases. To be more precise, in the screening process of the current study, a major part of potentially eligible cases had to be excluded due to missing DECT raw data.

In all patients with lymph node metastases the diagnosis was histologically confirmed and the segmented lymph nodes showed unequivocal metastatic involvement as defined by RECIST criteria. Yet, histologic confirmation was performed in a location that was clinically feasible to reach and may not be identical to the selected lymph nodes in our study.

Last, we restricted the patient inclusion to one dual-energy CT scanner to exclude inter-scanner variability and to include only reconstructions with a slice thickness of 1.5 mm and increment of 1.2 mm, nevertheless, intra-scanner variability may have occurred.

5. Conclusions

In conclusion, we could demonstrate that radiomics models were superior to DECT material decomposition in the objective identification of visually unequivocal abdominal lymph node metastases. Our study gives evidence that an automatic stratification of unequivocal lymph node metastases might be feasible using radiomics-based machine learning models. As the demand for medical imaging is steadily increasing, radiomics may serve as a prioritization support tool to help radiologists focus on equivocal and critical cases. In contrast to DECT material decomposition, high-performing artificial intelligence methodologies are applicable in standard-of-care CT images. Thus, quantitative imaging biomarkers are not restricted to medical institutions with DECT equipment.

Ethical statement

Ethical approval: We obtained institutional review board (IRB) approval of the Ethical Committee at the University Hospital Frankfurt (project-number: 20/688) and written informed consent was waived for this retrospective study. The patient population was not reported previously.

Funding statement

This research did not receive any specific grant from funding agencies in the public, commercial, or not-for-profit sectors.

CRediT authorship contribution statement

Scherwin Mahmoudi: Conceptualization, Data curation, Formal analysis, Investigation, Methodology, Project administration, Software, Supervision, Validation, Writing – original draft, Writing – review & editing. **Vitali Koch:** Data curation, Formal analysis, Methodology, Software, Validation, Writing – review & editing. **Daniel Pinto Dos Santos:** Conceptualization, Data curation, Formal analysis, Investigation, Methodology, Project administration, Software, Supervision, Validation, Visualization, Writing – review & editing. **Jörg Ackermann:** Formal analysis, Methodology, Software, Validation, Writing – review & editing. **Leon D. Grünewald:** Data curation, Formal analysis, Methodology, Validation, Writing – review & editing. **Inga Weitkamp:** Data curation, Methodology, Validation, Visualization, Writing – original draft. **Ibrahim Yel:** Data curation, Formal analysis, Methodology, Software, Validation, Writing – review & editing. **Simon S. Martin:** Data curation, Formal analysis, Investigation, Methodology, Software, Supervision, Validation, Visualization, Writing – review & editing. **Moritz Albrecht:** Conceptualization, Data curation, Formal analysis, Methodology, Project administration, Supervision, Validation, Writing – review & editing. **Jan-Erik Scholtz:** Conceptualization, Data curation, Formal analysis, Investigation, Methodology, Project administration, Software, Supervision, Validation, Visualization, Writing – review & editing. **Thomas J. Vogl:** Data curation, Formal analysis, Investigation, Methodology, Project administration, Resources, Software, Supervision, Validation, Visualization, Writing – review & editing. **Simon Bernatz:** Conceptualization, Data curation, Formal analysis, Investigation, Methodology, Project administration, Software, Supervision, Validation, Writing – original draft, Writing – review & editing.

Declaration of Competing Interest

The authors declare that they have no known competing financial interests or personal relationships that could have appeared to influence the work reported in this paper.

Appendix A. Supporting information

Supplementary data associated with this article can be found in the online version at doi:10.1016/j.ejro.2022.100459.

References

[1] J. Heijmans, S. Krausz, J.M. van Es, T.W. Kuijpers, G.J. de Bree, [Lymphadenopathy in general practice], Ned. Tijdschr. Geneeskd. 165 (2021).
[2] R.E. Dorfman, M.B. Alpern, B.H. Gross, M.A. Sandler, Upper abdominal lymph nodes: criteria for normal size determined with CT, Radiology 180 (1991) 319–322, https://doi.org/10.1148/radiology.180.2.2068292.

[3] E.A. Eisenhauer, P. Therasse, J. Bogaerts, L.H. Schwartz, D. Sargent, R. Ford, J. Dancey, S. Arbuck, S. Gwyther, M. Mooney, L. Rubinstein, L. Shankar, L. Dodd, R. Kaplan, D. Lacombe, J. Verweij, New response evaluation criteria in solid tumours: revised RECIST guideline (version 1.1), Eur. J. Cancer 45 (2009) 228–247, https://doi.org/10.1016/j.ejca.2008.10.026.
[4] T. Horn, T. Zahel, N. Adt, S.C. Schmid, M.M. Heck, M.K. Thalgott, G. Hatzichristodoulou, B. Haller, M. Autenrieth, H.R. Kübler, J.E. Gschwend, K. Holzapfel, T. Maurer, Evaluation of Computed Tomography for Lymph Node Staging in Bladder Cancer Prior to Radical Cystectomy, Urol. Int 96 (2016) 51–56, https://doi.org/10.1159/000440889.
[5] R.L. van Heertum, R. Scarimbolo, J.G. Wolodzko, B. Klencke, R. Messmann, F. Tunc, L. Sokol, R. Agarwal, J.A. Strafaci, M. O'Neal, Lugano 2014 criteria for assessing FDG-PET/CT in lymphoma: an operational approach for clinical trials. Drug Des. Devel Ther. 11 (2017) 1719–1728, https://doi.org/10.2147/DDDT.S136988.
[6] V. Markotić, T. Pojužina, D. Radančević, M. Miljko, V. Pokrajčić, The Radiologist Workload Increase; Where Is the Limit?: Mini Review and Case Study, Psychiatr. Danub 33 (2021) 768–770. ⟨http://www.ncbi.nlm.nih.gov/pubmed/34718316⟩. accessed April 9, 2022.
[7] F. Tatsugami, T. Higaki, Y. Nakamura, Y. Honda, K. Awai, Dual-energy CT: minimal essentials for radiologists, Jpn J. Radio. (2022), https://doi.org/10.1007/s11604-021-01233-2.
[8] C. Liguori, G. Frauenfelder, C. Massaroni, P. Saccomandi, F. Giurazza, F. Pitocco, R. Marano, E. Schena, Emerging clinical applications of computed tomography, Med Devices (Auckl.) 8 (2015) 265–278, https://doi.org/10.2147/MDER.S70630.
[9] H. Chandarana, A.J. Megibow, B.A. Cohen, R. Srinivasan, D. Kim, C. Leidecker, M. Macari, Iodine quantification with dual-energy CT: phantom study and preliminary experience with renal masses, AJR Am. J. Roentgenol. 196 (2011) W693–W700, https://doi.org/10.2214/AJR.10.5541.
[10] X. Li, X. Meng, Z. Ye, Iodine quantification to characterize primary lesions, metastatic and non-metastatic lymph nodes in lung cancers by dual energy computed tomography: An initial experience, Eur. J. Radio. 85 (2016) 1219–1223, https://doi.org/10.1016/j.ejrad.2016.03.030.
[11] S. Rizzo, D. Radice, M. Femia, P. De Marco, D. Origgi, L. Preda, M. Barberis, R. Vigorito, G. Mauri, A. Mauro, M. Bellomi, Metastatic and non-metastatic lymph nodes: quantification and different distribution of iodine uptake assessed by dual-energy CT, Eur. Radio. 28 (2018) 760–769, https://doi.org/10.1007/s00330-017-5015-5.
[12] R.J. Gillies, P.E. Kinahan, H. Hricak, Radiomics: Images Are More than Pictures, They Are Data, Radiology 278 (2016) 563–577, https://doi.org/10.1148/radiol.2015151169.
[13] S. Bedrikovetski, N.N. Dudi-Venkata, H.M. Kroon, W. Seow, R. Vather, G. Carneiro, J.W. Moore, T. Sammour, Artificial intelligence for pre-operative lymph node staging in colorectal cancer: a systematic review and meta-analysis, BMC Cancer 21 (2021) 1058, https://doi.org/10.1186/s12885-021-08773-w.
[14] M. Kirienko, G. Ninatti, L. Cozzi, E. Voulaz, N. Gennaro, I. Barajon, F. Ricci, C. Carlo-Stella, P. Zucali, M. Sollini, L. Balzarini, A. Chiti, Computed tomography (CT)-derived radiomic features differentiate prevascular mediastinum masses as thymic neoplasms versus lymphomas, Radio. Med 125 (2020) 951–960, https://doi.org/10.1007/s11547-020-01188-w.
[15] Y. Bian, S. Guo, H. Jiang, S. Gao, C. Shao, K. Cao, X. Fang, J. Li, L. Wang, C. Ma, J. Zheng, G. Jin, J. Lu, Radiomics nomogram for the preoperative prediction of lymph node metastasis in pancreatic ductal adenocarcinoma, Cancer Imaging 22 (2022) 4, https://doi.org/10.1186/s40644-021-00443-1.
[16] J. Li, M. Fang, R. Wang, D. Dong, J. Tian, P. Liang, J. Liu, J. Gao, Diagnostic accuracy of dual-energy CT-based nomograms to predict lymph node metastasis in gastric cancer, Eur. Radio. 28 (2018) 5241–5249, https://doi.org/10.1007/s00330-018-5483-2.
[17] Y. Liu, Y. Dou, F. Lu, L. Liu, A study of radiomics parameters from dual-energy computed tomography images for lymph node metastasis evaluation in colorectal mucinous adenocarcinoma, Medicine 99 (2020), e19251, https://doi.org/10.1097/MD.0000000000019251.
[18] C. An, D. Li, S. Li, W. Li, T. Tong, L. Liu, D. Jiang, L. Jiang, G. Ruan, N. Hai, Y. Fu, K. Wang, S. Zhuo, J. Tian, Deep learning radiomics of dual-energy computed tomography for predicting lymph node metastases of pancreatic ductal adenocarcinoma, Eur. J. Nucl. Med Mol. Imaging (2021), https://doi.org/10.1007/s00259-021-05573-z.
[19] P. Lambin, E. Rios-Velazquez, R. Leijenaar, S. Carvalho, R.G.P.M. Van Stiphout, P. Granton, C.M.L. Zegers, R. Gillies, R. Boellard, A. Dekker, H.J.W.L. Aerts, Radiomics: Extracting more information from medical images using advanced feature analysis, Eur. J. Cancer 48 (2012) 441–446, https://doi.org/10.1016/j.ejca.2011.11.036.
[20] V. Kumar, Y. Gu, S. Basu, A. Berglund, S.A. Eschrich, M.B. Schabath, K. Forster, H. J.W.L. Aerts, A. Dekker, D. Fenstermacher, D.B. Goldgof, L.O. Hall, P. Lambin, Y. Balagurunathan, R.A. Gatenby, R.J. Gillies, Radiomics: the process and the challenges, Magn. Reson Imaging 30 (2012) 1234–1248, https://doi.org/10.1016/j.mri.2012.06.010.
[21] A. Fedorov, R. Beichel, J. Kalpathy-Cramer, J. Finet, J.-C. Fillion-Robin, S. Pujol, C. Bauer, D. Jennings, F. Fennessy, M. Sonka, J. Buatti, S. Aylward, J. v. Miller, S. Pieper, R. Kikinis, 3D Slicer as an image computing platform for the Quantitative Imaging Network, Magn. Reson Imaging 30 (2012) 1323–1341, https://doi.org/10.1016/j.mri.2012.05.001.
[22] A. Zwanenburg, S. Leger, M. Vallières, S. Löck, Image biomarker standardisation initiative, arXiv. arXiv Prep. (2016), https://doi.org/10.17195/candat.2016.08.1.
[23] J.J.M. van Griethuysen, A. Fedorov, C. Parmar, A. Hosny, N. Aucoin, V. Narayan, R.G.H. Beets-Tan, J.-C. Fillion-Robin, S. Pieper, H.J.W.L. Aerts, Computational Radiomics System to Decode the Radiographic Phenotype, Cancer Res 77 (2017) e104–e107, https://doi.org/10.1158/0008-5472.CAN-17-0339.
[24] S. Bernatz, Y. Zhdanovich, J. Ackermann, I. Koch, P.J. Wild, D. Pinto, T.J. Vogl, B. Kaltenbach, N. Rosbach, Impact of rescanning and repositioning on radiomic features employing a multi-object phantom in magnetic resonance imaging, Sci. Rep. 11 (2021) 1–13, https://doi.org/10.1038/s41598-021-93756-x.
[25] P. Lambin, R.T.H. Leijenaar, T.M. Deist, J. Peerlings, E.E.C. de Jong, J. van Timmeren, S. Sanduleanu, R.T.H.M. Larue, A.J.G. Even, A. Jochems, Y. van Wijk, H. Woodruff, J. van Soest, T. Lustberg, E. Roelofs, W. van Elmpt, A. Dekker, F. M. Mottaghy, J.E. Wildberger, S. Walsh, Radiomics: the bridge between medical imaging and personalized medicine, Nat. Rev. Clin. Oncol. 14 (2017) 749–762, https://doi.org/10.1038/nrclinonc.2017.141.
[26] S. Bernatz, Y. Zhdanovich, J. Ackermann, I. Koch, P.J. Wild, D. Pinto, T.J. Vogl, B. Kaltenbach, N. Rosbach, Impact of rescanning and repositioning on radiomic features employing a multi-object phantom in magnetic resonance imaging, Sci. Rep. 11 (2021) 1–13, https://doi.org/10.1038/s41598-021-93756-x.
[27] R. Vallat, Pingouin: statistics in Python, J. Open Source Softw. 3 (2018) 1026, https://doi.org/10.21105/joss.01026.
[28] T. Kluyver, B. Ragan-Kelley, F. Pérez, B. Granger, M. Bussonnier, J. Frederic, K. Kelley, J. Hamrick, J. Grout, S. Corlay, P. Ivanov, D. Avila, S. Abdalla, C. Willing, J. D. Team, Jupyter Notebooks—a publishing format for reproducible computational workflows, Positioning and Power in Academic Publishing: Players, Agents and Agendas - Proceedings of the 20th International Conference on Electronic Publishing, ELPUB 2016. (2016) 87–90. https://doi.org/10.3233/978–1-61499–649-1–87.
[29] F. Pedregosa, G. Varoquaux, A. Gramfort, V. Michel, B. Thirion, O. Grisel, M. Bondel, P. Prettenhofer, R. Weiss, V. Dubourg, J. Vanderplas, A. Passos, D. Cournapeau, M. Brucher, M. Perrot, É. Duchesnay, Scikit-learn: Machine Learning in Python, J. Mach. Learn. Res. 12 (2011) 2825–2830.
[30] M.P.A. Starmans, S.R. Van Der Voort, T. Phil, M.J.M. Timbergen, M. Vos, A. Guillaume, W. Kessels, C. Verhoef, S. Sleijfer, M. Smits, R.S. Dwarkasing, C.J. Els, F. Fiduzi, A. Blazevic, T. Brabander, R.A.H. Van Gils, G.J.H. Franssen, R.A. Feelders, W.W. De Herder, E. Florian, B.G. Koerkamp, L. Angus, A.A.M. Van Der Veldt, A. Rajicic, A.E. Odink, M. Deen, J. Veenland, I. Schoots, M. Renckens, M. Doukas, A. De Man, R.L. Miclea, P.B. Vermeulen, E.E. Bron, M.G. Thomeer, J. Jacob, W.J. Niessen, S. Klein, Reproducible radiomics through automated machine learning validated on twelve clinical applications, (2021).
[31] X. Sun, W. Xu, Fast Implement. DeLong ' S. Algorithm Comp. Areas Correl. Receiv. 21 (2014) 1389–1393.
[32] J. Choe, M.Y. Kim, J.K. Yun, G.D. Lee, Y.-H. Kim, S. Choi, D.K. Kim, Sublobar Resection in Stage IA Non-Small Cell Lung Cancer: Role of Preoperative CT Features in Predicting Pathologic Lymphovascular Invasion and Postoperative Recurrence, AJR Am. J. Roentgenol. 217 (2021) 871–881, https://doi.org/10.2214/AJR.21.25618.
[33] S.E.M. Ven, L. Suzuki, A.W. Gotink, F.J.C. ten Kate, D. Nieboer, B.L.A.M. Weusten, L.A.A. Brosens, R. Hillegersberg, L. Alvarez Herrero, C.A. Seldenrijk, A. Alkhalaf, F. C.P. Moll, W. Curvers, I.G. Lijnschoten, T.J. Tang, H. Valk, W.B. Nagengast, G. Kats-Ugurlu, J.T.M. Plukker, M.H.M.G. Houben, J.S. Laan, R.E. Pouw, J.J.G.H. M. Bergman, S.L. Meijer, M.I. Berge Henegouwen, B.P.L. Wijnhoven, P.J.F. Jonge, M. Doukas, M.J. Bruno, K. Biermann, A.D. Koch, Lymphovascular invasion quantification could improve risk prediction of lymph node metastases in patients with submucosal (T1b) esophageal adenocarcinoma, U. Eur. Gastroenterol. J. 9 (2021) 1066–1073, https://doi.org/10.1002/ueg2.12151.
[34] Y. Inoue, Radiation Dose Modulation of Computed Tomography Component in Positron Emission Tomography/Computed Tomography, Semin Nucl. Med (2021), https://doi.org/10.1053/j.semnuclmed.2021.11.009.
[35] R. Doda Khera, F. Homayounieh, F. Lades, B. Schmidt, M. Sedlmair, A. Primak, S. Saini, M.K. Kalra, Can Dual-Energy Computed Tomography Quantitative Analysis and Radiomics Differentiate Normal Liver From Hepatic Steatosis and Cirrhosis? J. Comput. Assist Tomogr. 44 (2020) 223–229, https://doi.org/10.1097/RCT.0000000000000989.
[36] S. Ebrahimian, R. Singh, A. Netaji, K.S. Madhusudhan, F. Homayounieh, A. Primak, F. Lades, S. Saini, M.K. Kalra, S. Sharma, Characterization of Benign and Malignant Pancreatic Lesions with DECT Quantitative Metrics and Radiomics, Acad. Radio. (2021), https://doi.org/10.1016/j.acra.2021.07.008.
[37] F. Homayounieh, R. Singh, C. Nitiwarangkul, F. Lades, B. Schmidt, M. Sedlmair, S. Saini, M.K. Kalra, Semiautomatic Segmentation and Radiomics for Dual-Energy CT: A Pilot Study to Differentiate Benign and Malignant Hepatic Lesions, AJR Am. J. Roentgenol. 215 (2020) 398–405, https://doi.org/10.2214/AJR.19.22164.
[38] R. Doda Khera, F. Homayounieh, F. Lades, B. Schmidt, M. Sedlmair, A. Primak, S. Saini, M.K. Kalra, Can Dual-Energy Computed Tomography Quantitative Analysis and Radiomics Differentiate Normal Liver From Hepatic Steatosis and Cirrhosis? J. Comput. Assist Tomogr. 44 (2020) 223–229, https://doi.org/10.1097/RCT.0000000000000989.
[39] S. Rizzo, D. Radice, M. Femia, P. De Marco, D. Origgi, L. Preda, M. Barberis, R. Vigorito, G. Mauri, A. Mauro, M. Bellomi, Metastatic and non-metastatic lymph nodes: quantification and different distribution of iodine uptake assessed by dual-energy CT, Eur. Radio. 28 (2018) 760–769, https://doi.org/10.1007/s00330-017-5015-5.
[40] X. Li, X. Meng, Z. Ye, Iodine quantification to characterize primary lesions, metastatic and non-metastatic lymph nodes in lung cancers by dual energy

computed tomography: An initial experience, Eur. J. Radio. 85 (2016) 1219–1223, https://doi.org/10.1016/j.ejrad.2016.03.030.

[41] J. Yang, L. Wang, J. Qin, J. Du, M. Ding, T. Niu, R. Li, Multi-view learning for lymph node metastasis prediction using tumor and nodal radiomics in gastric cancer, Phys. Med Biol. (2022), https://doi.org/10.1088/1361-6560/ac515b.

[42] C. An, D. Li, S. Li, W. Li, T. Tong, L. Liu, D. Jiang, L. Jiang, G. Ruan, N. Hai, Y. Fu, K. Wang, S. Zhuo, J. Tian, Deep learning radiomics of dual-energy computed tomography for predicting lymph node metastases of pancreatic ductal adenocarcinoma, Eur. J. Nucl. Med Mol. Imaging (2021), https://doi.org/10.1007/s00259-021-05573-z.